Beampattern and Robust Doppler Filter Design for Spatial Modulation Based Joint RadCom Systems

Jifa Zhang

***Abstract*—Joint radar and communication (RadCom) systems have been proposed to achieve the spectrum sharing between radar and communication in recent years. However, the joint RadCom systems cause the clutter modulation and the performance degradation of both radar and communication. As a consequence, it's very critical to improve the performance of both radar and communication when designing joint RadCom systems. Firstly, this paper designs the constant modulus dual function waveforms for spatial modulation based joint RadCom systems. In order to solve the nonsmooth and nonconvex optimization problem, we propose a method based on alternating direction method of multipliers (ADMM) to obtain a suboptimal solution. Secondly, this paper analyses the effect of beampattern variation on clutter modulation for spatial modulation based joint RadCom systems. Besides, this paper considers the design of robust doppler filter for joint RadCom systems when the receive temporal steering vector is mismatched to the desired temporal steering vector. This paper aims to maximize the worst signal-to-interference-plus-noise-ratio (SINR) of the doppler filter in the specific doppler interval under the similarity constraint and constant white noise gain constraint. In order to solve the nonconvex optimization problem, we relax the original optimization problem to a semidefinite programming (SDP), which is convex and can be solved using off-the-shelf optimization solvers. What's more, the rank-one decomposition method is utilized to synthesize the weight vector of the proposed robust doppler filter. Finally, lots of simulation results are presented to show the robustness of the designed doppler filter.**

***Index Terms*—Beampattern design, Constant modulus, Robust doppler filter design, Joint RadCom systems, Spatial modulation, SemiDefinite programming.**

I. INTRODUCTION

JOINT RadCom systems, where the radar and communication share the same hardware platform and the spectrum, have been proposed in recent years to alleviate fierce competition for scarce spectrum resources from radar and communication [1]–[4]. The joint RadCom systems have the advantages of low cost, compact size, safety and so on. As a consequence, there are many applications for joint RadCom systems, such as autonomous vehicles [5], [6], Internet of Things (IoT), and defence.

As for the joint RadCom systems where the radar is regraded as the primary function and communication is regarded as the secondary function, the main challenge is how to embed the communication symbols into the radar emission without degrading the performance of the radar [7]. Recently, lots of information embedding strategies have been proposed, such as index modulation [8]–[12], spatial modulation [13]–[16] and fast time modulation [17]–[19]. Spatial modulation embeds the communication information into the radar beampattern towards the communication direction while keeping the beampattern in the mainlobe unchanged. The essence of the spatial modulation is to steer the mainbeam towards the target of interest while allowing for controlled variations in the sidelobe region. The index modulation imbeds the communication information into the specific antenna index or frequency index. And the communication information is represented by specific radar waveforms for fast time modulation, such as waveform diversity. The waveforms of joint RadCom systems based on index modulation and fast time modulation are usually constant modulus, but the waveforms of spatial modulation based joint RadCom systems are usually inconstant modulus. However, the constant waveforms are very significant, since the radar amplifiers usually work in saturation conditions and the amplitude modulation (AM) may be difficult [20]. As a consequence, the constant waveforms design has received many researchers' attention in recent years [21], [22]. To the best of our knowledge, the constant modulus waveform design for spatial modulation based joint RadCom systems has not been studied. As a result, we design the beamforming weight vectors for spatial modulation based joint RadCom systems under constant modulus constraint in this paper.

In order to embed communication information into the radar emission, the joint RadCom systems inevitably introduce variations in radar waveforms or beampatterns for different pulses during a coherent pulse interval (CPI), which causes the clutter modulation and the performance degradation of the radar [23]. Therefore, it's critical to solve the clutter modulation problem and improve the performance of the radar. A joint least squares (JLS) mismatch filter was proposed to achieve nearly identical range sidelobe responses [24]. Different from the waveform diversity, the spatial modulation modulates the clutter located in different range and azimuth with different scale. In order to analyse the effect of clutter, knowledge-aid radar systems [25]–[29] where the radar systems have access to a dynamic environmental database, including a geographical information system (GIS), tracking files, meteorological information and interference models, have been proposed recently. In [26], the authors designed the robust doppler filter considering the uncertainties both in the receive useful signal component and interference covariance matrix. In [28], the authors considers the doppler robust design of transmit sequence and receive filter. Joint design radar transmit waveform and receive doppler filter bank can achieve higher output SINR. In [27], the authors assumed the doppler frequency shift of the target is unknown and maximized the worst SINR of the doppler filter bank by

Jifa Zhang is with the School of Electronic and Information Engineering, Beihang University, Beijing 100191, China, E-mail: (jifazhang@yeah.net)

jointly optimizing the radar waveform and receive filter bank via generalized fractional programming (GFP). In [29], the authors proposed an effective method to solve the max-min optimization problem to maximize the worst SINR. Different from the coded radar waveform, it's impossible to optimize the communication sequence, since the communication sequence is random in order to deliver the communication information. The authors in [30] analysed the effect of spatial modulation on stationary clutter mitigation and proposed a calibrated matched filter based on subspace projection. However, the ground reflection coefficients are assumed to be constant for each range cell and the doppler frequency of the ground clutter is assumed as zero which is usually not satisfied in practice. To the best of our knowledge, there is no existing work in the literature designing the robust doppler filter for spatial modulation based joint RadCom systems under more general clutter situation, which motivates our work.

In this paper, we design the constant modulus dual function waveforms for spatial modulation based joint RadCom systems, firstly. And then, we analyze the effect of spatial modulation on clutter mitigation of joint RadCom systems under the range ambiguous case, i.e., the clutter returns from multiple range rings compete with potential targets in the cell under test (CUT). What's more, the clutter reflection coefficients are assumed to obey the gaussian distribution. Although the doppler frequency of the target is known as prior information, considering the doppler frequency mismatch due to all kinds of reasons, we aim to design the robust doppler filter to maximize the worst SINR of the doppler filter in a specific doppler frequency interval.

The contributions of this paper are listed as below:

- First, we design the beamforming weight vectors for jspatial modulation based joint RadCom systems considering constant modulus constraint. What's more, we propose a method based on ADMM to solve the nonconvex and nonsmooth optimization problem.
- Next, we analyse the clutter modulation of joint RadCom systems based on spatial modulation under range ambiguous situation and derive the clutter covariance matrix.
- Furthermore, we consider the case of doppler frequency mismatch and aim to design the robust doppler filter for joint RadCom systems to maximize the worst SINR of the doppler filter in a specific doppler frequency interval. The original nonconvex optimization problem is relaxed to a SDP to obtain a suboptimal solution.

The reminder of this paper is organized as below. Section II describes the signalling strategy and beampattern design for spatial modulation based joint RadCom systems. The signal model is presented in Section III. The formulation of the proposed robust doppler filter is described in Section IV. The synthesis stage is described in Section V and simulation results are presented in Section VI. Finally, this paper is concluded in Section VII.

Notations: In this paper, the matrices and vectors are denoted by bold uppercase letters (i.e. $\mathbf{A}$) and lowercase letters (i.e. $\mathbf{a}$), respectively. And the scalars are denoted by normal font (i.e. σ). The transpose and the conjugate operation are $(\cdot)^T$ and $(\cdot)^H$, respectively. $\odot$ denotes the Hadamard element-wise product. $\mathbb{C}^N$ denotes the set of N-dimensional vectors of complex numbers. $\mathbf{I}$ denotes the identity matrix, whose dimension is determined by the context. $\mathbb{E}\{\cdot\}$ denotes the mathematical expectation, $|\cdot|$ denotes the module of a complex number and a^* denotes the conjugate of a. $\text{diag}\{\mathbf{b}\}$ denotes the diagonal matrix whose i-th diagonal element is the i-th entry of $\mathbf{b}$. $\Re(\cdot)$ denotes the real part of a complex number and $\|\mathbf{x}\|$ denotes the Euclidean norm of the vector $\mathbf{x}$. $\text{tr}(\cdot)$ denotes the trace of the matrix argument and $\text{rank}(\mathbf{A})$ denotes the rank of $\mathbf{A}$. For any hermitian matrix $\mathbf{A}$, $\mathbf{A} \succeq \mathbf{0}$ and $\mathbf{A} \succ \mathbf{0}$ denotes $\mathbf{A}$ is a positive semidefinite matrix and positive definite matrix, respectively. $\nu(\mathcal{P})$ denotes the optimal value for any optimization problem $\mathcal{P}$. $\mathbf{B}^{-1}$ denotes the inverse matrix of the invertible matrix $\mathbf{B}$. $arg\max$ stands for the argument of the maximum. $\text{mod}(a, m)$ returns the remainder after division of a by m. j denotes the imaginary unit. $\mathbb{R}$ denotes the field of all real numbers. $\text{range}(\mathbf{W})$ denotes the range space of $\mathbf{W}$.

II. SIGNALLING STRATEGY AND BEAMPATTERN DESIGN FOR SPATIAL MODULATION

The AM signalling strategy, which modulates sidelobe level of the transmit beampatterns towards the communication direction, is the generalized mathematical formulation of existing spatial modulation techniques in joint RadCom systems. As for the AM signalling strategy, the communication symbols are represented by the specific sidelobe levels towards the communication direction and the beampattern in the mainlobe is desired to be unchanged.

Suppose a joint RadCom platform which is equipped with a M-element uniform linear array (ULA) with inter-element spacing of half wavelength for transmit and an omnidirectional antenna for receive [31]. Assuming L bits communication information are embedded in each pulse, the number of communication symbols is $K = 2^L$. In the literature, the constant modulus waveforms for spatial modulation based joint RadCom systems has not been studied, which motivates our work.

We aim to minimize the peak sidelobe level (PSL) and keep the specific level towards the target of interest and the communication receiver under the constant modulus constraint. The kth beamforming weight vectors for the AM-based signalling strategy can be obtained by solving the following optimization problem [18]:

$$\begin{aligned} \min_{\mathbf{h}_k} \quad & \max_{i=1,\cdots,I} |\mathbf{h}_k^H \mathbf{a}(\theta_i)|^2 \quad \theta_i \in \bar{\mathbf{\Theta}} \\ \text{subject to} \quad & \mathbf{h}_k^H \mathbf{a}(\theta_t) = 1 \\ & \mathbf{h}_k^H \mathbf{a}(\theta_c) = \Delta_k \\ & |\mathbf{h}_k(m)| = 1, \quad m = 1, \cdots, M \end{aligned} \tag{1}$$

where $\theta_i \, (i = 1, \cdots, I)$ denotes the finite angle grid in the radar sidelobe region, $\bar{\mathbf{\Theta}}$ denotes the radar sidelobe region, Δ_k denotes the predefined sidelobe level towards the communication direction, θ_t is the direction of the target of interest, θ_c denotes the direction of the communication receiver and $\mathbf{h}_k \in \mathbb{C}^M$ is the k-th beamforming weight vector to form the beampattern whose sidelobe level towards the communication

receiver is Δ_k. Every sidelobe level Δ_k is chosen from the predefined dictionary $\mho = \{\Delta_1, \Delta_2, \cdots, \Delta_K\}$ containing K different sidelobe levels. The constraint $|\mathbf{h}_k(m)| = 1\,(m = 1, 2, \cdots, M)$ grantees the constant modulus of the radar waveforms.

However, the optimization problem (1) is nonconvex and nonsmooth, since the constraint $|\mathbf{h}_k(m)| = 1\,(m = 1, 2, \cdots, M)$ denotes a nonconvex set and the objective function is nonsmooth. Therefore, the problem is a NP-hard problem and it's very difficult to solve the optimization problem. In order to solve this nonconvex optimization problem, we propose a method based on ADMM to obtain a suboptimal solution. We introduce auxiliary variables $\{\varsigma_i\}$, $\mathbf{z}_k \in \mathbb{C}^M$ and $\rho \in \mathbb{R}$ to transform optimization problem (1) to a smooth optimization problem, and (1) can be recast equivalently as

$$\begin{aligned} \min \quad & \rho^2 \\ \text{subject to } & |\varsigma_i| \le \rho, \quad i = 1, \cdots, I \\ & \varsigma_i = \mathbf{h}_k^H \mathbf{a}(\theta_i), \quad i = 1, \cdots, I \\ & \mathbf{h}_k^H \mathbf{a}(\theta_l) = \Delta_l, \quad l = 1, 2 \\ & \mathbf{h}_k(m) = \mathbf{z}_k(m), \quad m = 1, \cdots, M \\ & |\mathbf{z}_k(m)| = 1, \quad m = 1, \cdots, M \end{aligned} \tag{2}$$

where ρ denotes the upper bound of the PSL, $\Delta_1 = 1, \Delta_2 = \Delta_k$ and θ_l $(l = 1, 2)$ are the angles of the target of interest and communication receiver, respectively.

The augmented Lagrangian function for (2) is given by (3) at the top of the next page where λ_i, μ_l, ν_m are Lagrangian multipliers and $\varrho_g > 0\,(g = 1, 2, 3)$ are penalty parameters.

Let $\mathbf{h}_k^\ell$ denotes the value of $\mathbf{h}_k$ at ℓ-th iteration. And the symbol naming rule apply to other variables. The iteration rule of proposed method based on ADMM can be formulated as below:

$$\begin{aligned} \{\rho^{\ell+1}, \{\varsigma_i^{\ell+1}\}\} = \arg min\ & \mathcal{L}(\rho, \{\varsigma_i\}, \{\mathbf{h}_k^\ell\}, \{\mathbf{z}_k^\ell\}, \\ & \{\lambda_i^\ell\}, \{\mu_l^\ell\}, \{\nu_m^\ell\}) \\ & \text{subject to } |\varsigma_i| \le \rho, \quad i = 1, \cdots, I \end{aligned} \tag{4}$$

$$\begin{aligned} \{\mathbf{h}_k^{\ell+1}\} = \arg min\ & \mathcal{L}(\rho^{\ell+1}, \{\varsigma_i^{\ell+1}\}, \{\mathbf{h}_k\}, \{\mathbf{z}_k^\ell\} \\ & , \{\lambda_i^\ell\}, \{\mu_l^\ell\}, \{\nu_m^\ell\}) \end{aligned} \tag{5}$$

$$\begin{aligned} \{\mathbf{z}_k^{\ell+1}\} = \arg min\ & \mathcal{L}(\rho^{\ell+1}, \{\varsigma_i^{\ell+1}\}, \{\mathbf{h}_k^{\ell+1}\}, \{\mathbf{z}_k\}, \\ & \{\lambda_i^\ell\}, \{\mu_l^\ell\}, \{\nu_m^\ell\}) \\ & \text{subject to } |\mathbf{z}_k(m)| = 1, \quad m = 1, \cdots, M \end{aligned} \tag{6}$$

$$\lambda_i^{\ell+1} = \lambda_i^\ell + \beta\varrho_1(\varsigma_i^{\ell+1} - \mathbf{h}_k^{(\ell+1)H}\mathbf{a}(\theta_i)) \tag{7}$$

$$\mu_l^{\ell+1} = \mu_l^\ell + \beta\varrho_2(\mathbf{h}_k^{(\ell+1)H}\mathbf{a}(\theta_l) - \Delta_l) \tag{8}$$

$$\nu_m^{\ell+1} = \nu_m^\ell + \beta\varrho_3(\mathbf{h}_k^{\ell+1}(m) - \mathbf{z}_k^{\ell+1}(m)) \tag{9}$$

where $\beta \ge 0$ denotes the dual step size. ρ, $\{\varsigma_i\}$, $\mathbf{h}_k$, $\mathbf{z}_k$ are primary variables and λ_i, μ_l, ν_m are dual variables.

In next subsections, we analyze the sub-optimization problems (4), (5) and (6), respectively. For notational simplicity, we omit the superscript of the variables, i.e., ρ^ℓ is replaced by ρ.

A. Solving Subproblem (4)

The subproblem (4) can be formulated as

$$\begin{aligned} \min_{\{\varsigma_i\}, \rho} \quad & \varrho_1 \sum_{i=1}^{I} |\varsigma_i|^2 + \Re\left[\sum_{i=1}^{I} (\lambda_i - \varrho_1 \mathbf{a}^H(\theta_i)\mathbf{h}_k)^* \varsigma_i\right] + \rho^2 \\ \text{subject to } \quad & |\varsigma_i| \le \rho, \quad \forall i \end{aligned} \tag{10}$$

Let $f(\varsigma_1, \cdots, \varsigma_I, \rho) \triangleq \varrho_1 \sum_{i=1}^{I} |\varsigma_i|^2 + \Re[\sum_{i=1}^{I} (\lambda_i - \varrho_1 \mathbf{a}^H(\theta_i)\mathbf{h}_k)^* \varsigma_i] + \rho^2$, the Hessian matrix can be formulated as

$$\mathbf{\Psi} = \begin{bmatrix} 2\varrho_1 & & & & \\ & 2\varrho_1 & & & \\ & & \ddots & & \\ & & & 2\varrho_1 & \\ & & & & 2 \end{bmatrix}. \tag{11}$$

The Hessian matrix $\mathbf{\Psi}$ is a positive definite matrix, therefore, the objective function is convex. What's more, the constraints are all convex. Therefore, the subproblem (10) is convex and can be solved using off-the-shelf optimization solvers, such as CVX.

B. Solving Subproblem (5)

The subproblem (5) can be formulated as

$$\min_{\mathbf{h}_k} \quad \mathbf{h}_k^H \mathbf{D} \mathbf{h}_k + \Re[\mathbf{e}^H \mathbf{h}_k] \tag{12}$$

where $\mathbf{e}$ and $\mathbf{D}$ can be formulated as

$$\begin{aligned} \mathbf{e} = & \sum_{i=1}^{I} -\lambda_i^* \mathbf{a}(\theta_i) + \sum_{l=1}^{2} \mu_l^* \mathbf{a}(\theta_l) + \boldsymbol{\nu} \\ & - \sum_{i=1}^{I} \varrho_1(\varsigma_i^* \mathbf{a}(\theta_i)) - \sum_{l=1}^{2} \varrho_2(\mathbf{a}(\theta_l)\Delta_l) - \varrho_3 \mathbf{z}, \\ \mathbf{D} = & \frac{\varrho_1}{2} \sum_{i=1}^{I} \mathbf{a}(\theta_i)\mathbf{a}^H(\theta_i) + \frac{\varrho_2}{2} \sum_{l=1}^{2} \mathbf{a}(\theta_l)\mathbf{a}^H(\theta_l) + \frac{\varrho_3}{2}\mathbf{I}, \end{aligned} \tag{13}$$

where $\boldsymbol{\nu} = [\nu_1, \nu_2, \cdots, \nu_M]^T$.

Since the matrix $\mathbf{D}$ is a positive definite matrix, the optimization (12) is convex, and the optimal solution can be formulated as $\tilde{\mathbf{h}}_k = -\frac{1}{2}\mathbf{D}^{-1}\mathbf{e}$.

C. Solving Subproblem (6)

The subproblem (6) can be formulated as

$$\begin{aligned} \min_{\mathbf{z}} \quad & \Re[\mathbf{y}^H \mathbf{z}] \\ \text{subject to } & |\mathbf{z}(m)| = 1, \quad \forall m \end{aligned} \tag{14}$$

where $\mathbf{y} = (-\boldsymbol{\nu} - \varrho_3 \mathbf{h}_k)$. Suppose $\mathbf{y}^*(m) = \epsilon(\cos(\phi) + j\sin(\phi))$, the corresponding optimal solution can be formulated as [21]

$$\tilde{\mathbf{z}}(m) = \begin{cases} \cos(\pi - \phi) + j\sin(\pi - \phi), & \text{if } \phi \ge 0 \\ \cos(-\pi - \phi) + j\sin(-\pi - \phi), & \text{otherwise.} \end{cases} \tag{15}$$

$$\mathcal{L} = \rho^2 + \Re\left[\sum_{i=1}^{I} \lambda_i^H(\varsigma_i - \mathbf{h}_k^H \mathbf{a}(\theta_i))\right] + \Re\left[\sum_{l=1}^{2} \mu_l^H(\mathbf{h}_k^H \mathbf{a}(\theta_l) - \Delta_l)\right] + \Re\left[\sum_{m=1}^{M} \nu_m^H(\mathbf{h}_k(m) - \mathbf{z}_k(m))\right] \tag{3}$$
$$+ \frac{\varrho_1}{2}\sum_{i=1}^{I} |\varsigma_i - \mathbf{h}_k^H \mathbf{a}(\theta_i)|^2 + \frac{\varrho_2}{2}\sum_{l=1}^{2} |\mathbf{h}_k^H \mathbf{a}(\theta_l) - \Delta_l|^2 + \frac{\varrho_3}{2}\sum_{m=1}^{M} |\mathbf{h}_k(m) - \mathbf{z}_k(m)|^2$$

D. Algorithm description

In practice, the constraint $\mathbf{h}_k^H \mathbf{a}(\theta_l) = \Delta_l$ and $\mathbf{h}_k(m) = \mathbf{z}_k(m)$ is hard to be satisfied. Therefore, we have to update ϱ_2 and ϱ_3 in each iteration to satisfy the equation as much as possible .

We update ϱ_2 when $|\mathbf{h}_k^H \mathbf{a}(\theta_l) - \Delta_l| > \gamma_1$, which can be formulated as

$$\varrho_2 = \max(20, \min(1.4 \times (\ell + 1), 6 \times 10^3)) \tag{16}$$

When $|\mathbf{h}_k^l(m) - \mathbf{z}_k^l(m)| > \gamma_2$ and

$$|\mathbf{h}_k^{\ell+1}(m) - \mathbf{h}_k^{\ell}(m)| + |\mathbf{z}_k^{\ell+1}(m) - \mathbf{z}_k^{\ell}(m)| < |\mathbf{h}_k^{\ell}(m) - \mathbf{z}_k^{\ell}(m)|, \tag{17}$$

we update ϱ_3 as below

$$\varrho_3 = \max(20, \min(3 \times (\ell + 1), 10^6)) \tag{18}$$

We update the dual variables λ_i, μ_l and ν_m when ℓ is even. The detailed description of proposed method based on ADMM is shown in Algorithm 1.

Algorithm 1 Iteration algorithm based on ADMM

Input: γ_1, γ_2, η, $G = 2 \times 10^4$, $\ell = 0$, $\varrho_1 = 200$, $\varrho_2 = 20$, $\varrho_3 = 20$, $\eta = 10^{-2}$;
Output: $\mathbf{h}_k$;

```
Initiation
repeat
    ρ, {ς_i}, h_k and z_k update by (4), (5), (6);
    if mod(ℓ, 2) = 0 then
        λ_i, μ_l and ν_m update by (7), (8), (9);
    end if
    if |h_k^H a(θ_l) − Δ_l| > γ_1 then
        ϱ_2 = max(20, min(1.4 × (ℓ + 1), 6 × 10^3));
    end if
    if (17) is true then
        ϱ_3 = max(20, min(3 × (ℓ + 1), 10^6));
    end if
    ℓ = ℓ + 1;
until the changes in primary and dual variables are less than a given threshold η or reaches the maximum iteration number G;
```

III. SIGNAL MODEL

A. Slow time signal model

Consider the joint RadCom platform transmits a burst of N slow-time pulses in a CPI. The transmit weight matrix $\mathbf{H} = [\mathbf{h}_1, \mathbf{h}_2, \cdots, \mathbf{h}_N] \in \mathbb{C}^{M \times N}$ modulate the radar pulses. Each column vector of $\mathbf{H}$ is chosen from the set containing K vectors obtained by solving the optimization problem (1). We consider a far-field moving point-like target in this paper. The slow-time observation vector received by the single omnidirectional antenna in a CPI can be formulated as [29], [32]

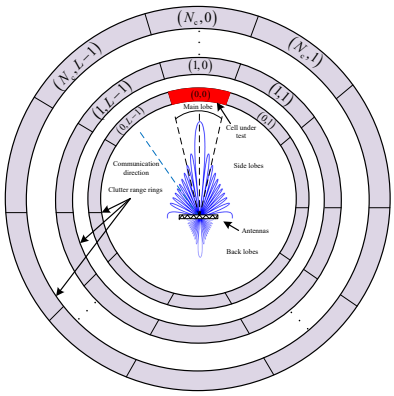

Fig. 1. Range-azimuth bins of illuminated area around radar antenna pattern.

$$\mathbf{x} = \alpha_t(\mathbf{H}^H \mathbf{a}(u_t)) \odot \mathbf{d}(\psi_t) + \mathbf{c} + \mathbf{n} \tag{19}$$
$$= \alpha_t \mathbf{s} \odot \mathbf{d}(\psi_t) + \mathbf{c} + \mathbf{n},$$

where α_t denotes the complex scattering coefficient of the target of interest, $\mathbf{s} \triangleq \mathbf{H}^H \mathbf{a}(u_t)$, $\mathbf{a}(u_t) = [1, e^{-j2\pi \frac{d}{\lambda} u_t}, \cdots, e^{-j2\pi(M-1)\frac{d}{\lambda} u_t}]^T \in \mathbb{C}^M$ is the spatial steering vector of the target of interest, λ denotes the wavelength, d is array element spacing, $u_t = sin(\theta_t)$ denotes the target electrical angle, $\mathbf{d}(\psi_t) = [1, e^{j2\pi\psi_t}, e^{j2\pi(2\psi_t)}, \cdots, e^{j2\pi(N-1)\psi_t}]^T \in \mathbb{C}^N$ denotes the temporal steering vector, $\psi_t = f_{d/t} T$ is the normalized target doppler frequency with $f_{d/t}$ the actual target doppler frequency and T the pulse repetition interval (PRI). The $N \times 1$ vector $\mathbf{n}$ denotes signal-independent noise samples which is modeled as zero-mean random vector with independent and identically distributed (IID) entries, i.e., $\mathbb{E}\{\mathbf{n}\} = \mathbf{0}$ and $\mathbb{E}\{\mathbf{n}\mathbf{n}^H\} = \sigma_n^2 \mathbf{I}$. σ_n^2 denotes the power of the noise.

In this paper, we consider the range ambiguous case, i.e., the clutter returns from multiple range rings competes with the potential target in the CUT as shown in Fig. 1. The clutter vector $\mathbf{c}$ can be formulated as [33]

$$\mathbf{c} = \sum_{r=1}^{N_c - 1} \sum_{i=0}^{L-1} \alpha_{(r,i)} \mathbf{J}_r(\mathbf{b}(u_i) \odot \mathbf{d}(\psi_{(r,i)})) \tag{20}$$
$$+ \sum_{i=0}^{L-1} \alpha_{(0,i)} \mathbf{b}(u_i) \odot \mathbf{d}(\psi_{(0,i)}),$$

where $\mathbf{b}(u_i) = \mathbf{H}^H \mathbf{a}(u_i) \in \mathbb{C}^N$ denotes the complex beampattern of N pulses, $N_c \leq N$ denotes the number of range

rings that interfere with the target of interest located in range-azimuth bin $(0,0)$, L denotes the number of discrete clutter patches in each clutter range ring, $\alpha_{(r,i)}$ and $\psi_{(r,i)}$ denotes the complex scattering coefficient and normalized doppler frequency of the clutter patches located in range-azimuth bin (r,i), and $\mathbf{J}_r \in \mathbb{C}^{N\times N}$ is the shift matrix which can be formulated as

$$\mathbf{J}_r(l_1,l_2)=\begin{cases}1, & \text{if } l_1-l_2=r\\ 0, & \text{otherwise}\end{cases} \quad (l_1,l_2)\in\{1,\dots,N\}^2 \tag{21}$$

When there is no information embedding in the radar pulses, the values of complex beampattern keep identical over N pulses and $\mathbf{c}$ can be rewritten as

$$\begin{aligned}\mathbf{c}=&\sum_{r=1}^{N_c-1}\sum_{i=0}^{L-1}\alpha_{(r,i)}\mathbf{J}_r(\delta_i\mathbf{d}(\psi_{(r,i)}))\\ &+\sum_{i=0}^{L-1}\alpha_{(0,i)}(\delta_i\mathbf{d}(\psi_{(0,i)})),\end{aligned} \tag{22}$$

where $\delta_i=\mathbf{h}_1^H\mathbf{a}(u_i)$ denotes the complex beampattern towards u_i.

However, when spatial modulation is utilized to embed communication symbols, the complex beampattern changes over different pulses causing the clutter modulation and the spreading of the clutter spectrum. We need to design the doppler filter to adapt to the modulated waveforms.

B. Clutter covariance matrix

We assume the complex scattering coefficients of different clutter range-azimuth bins are uncorrelated and obey to zero mean gaussian distribution, i.e., $\mathbb{E}\{\alpha_{(r,i)}\}=0$ and $\mathbb{E}\{|\alpha_{(r,i)}|^2\}=\sigma^2_{(r,i)}$ denotes the clutter power of clutter patch located in range-azimuth bin (r,i). Without loss of generality, we assume that the clutter power of clutter patches located in the same range ring are same, i.e.,

$$\sigma^2_{(r,0)}=\sigma^2_{(r,1)}=\cdots=\sigma^2_{(r,L-1)}=\sigma^2_r,\ r=0,\cdots,N_c-1 \tag{23}$$

and σ_r^2 can be formulated as [25]

$$\sigma_r^2=\sigma_0 K_r \tag{24}$$

where σ_0 can be estimated and K_r is a constant accounting for the channel propagation effects, such as additional system losses and the free space two-way path loss.

We assume the normalized doppler frequency of clutter patch located in range-azimuth bin (r,i) is uniformly distributed around a mean normalized doppler frequency $\bar{\psi}_{(r,i)}$ in normalized doppler interval $[\bar{\psi}_{(r,i)}-\frac{\epsilon_{(r,i)}}{2},\bar{\psi}_{(r,i)}+\frac{\epsilon_{(r,i)}}{2}]$, where $\epsilon_{(r,i)}$ denotes the interval length, i.e., $\psi_{(r,i)}\sim\mathcal{U}(\bar{\psi}_{(r,i)}-\frac{\epsilon_{(r,i)}}{2},\bar{\psi}_{(r,i)}+\frac{\epsilon_{(r,i)}}{2})$. Therefore, the covariance matrix of clutter vector $\mathbf{c}$ can be formulated in (25) at the top of next page, where $\Gamma(\mathbf{b}(u_i),(r,i)) = \text{diag}\{\mathbf{b}(u_i)\}\Phi_{\epsilon_{(r,i)}}^{\bar{\psi}_{(r,i)}}\text{diag}\{\mathbf{b}(u_i)\}^H$ with

$$\begin{aligned}\Phi_{\epsilon}^{\bar{\psi}}(l_1,l_2)&=\mathbb{E}\{e^{j2\pi(l_1-l_2)\psi}\}\\ &=\int_{\bar{\psi}-\frac{\epsilon}{2}}^{\bar{\psi}+\frac{\epsilon}{2}}e^{j2\pi(l_1-l_2)\psi}\frac{1}{\epsilon}d\psi\\ &=\begin{cases}1, & \text{if } l_1=l_2\\ e^{j2\pi\bar{\psi}(l_1-l_2)}\frac{sin[\pi\epsilon(l_1-l_2)]}{[\pi\epsilon(l_1-l_2)]}, & \text{otherwise.}\end{cases}\end{aligned} \tag{26}$$

The output SINR of the doppler filter can be formulated as [34]

$$\begin{aligned}\text{SINR}(\psi_q)&=\frac{|\alpha_t|^2|\mathbf{w}^H(\mathbf{s}\odot\mathbf{d}(\psi_q))|^2}{\mathbf{w}^H\mathbf{R}_c\mathbf{w}+\sigma_n^2\|\mathbf{w}\|^2}\\ &=\frac{|\alpha_t|^2|\mathbf{w}^H(\mathbf{s}\odot\mathbf{d}(\psi_q))|^2}{\mathbf{w}^H(\mathbf{R}_c+\sigma_n^2\mathbf{I})\mathbf{w}}\end{aligned} \tag{27}$$

where $\mathbf{w}\in\mathbb{C}^N$ denotes the doppler filter weight vector and $\psi_q\in\Omega, q=1,\cdots,Q$ denotes the discrete normalized doppler frequency in the doppler frequency interval of interest Ω.

IV. PROBLEM FORMULATION

In this paper, we assume that the parameters of the clutter are known by a dynamic environmental database. The output SINR is regarded as a measure of the receive filter performance. Although the desired temporal steering vector of the target of interest is known as prior information, the receive temporal steering vector is usually mismatched due to all kinds of reasons in practice. As a consequence, we aim to design a robust doppler receive filter to maximize the worst SINR in a specific doppler interval of interest Ω under similarity constraint and constant white noise gain constraint. The optimization problem of robust doppler receive filter for joint RadCom systems can be formulated as the below max-min optimization problem

$$\mathcal{P}\begin{cases}\max_{\mathbf{w}} & \min_{q=1,2,\cdots,Q}\ \frac{|\alpha_t|^2|\mathbf{w}^H(\mathbf{s}\odot\mathbf{d}(\psi_q))|^2}{\mathbf{w}^H\mathbf{R}_c\mathbf{w}+\sigma_n^2\|\mathbf{w}\|^2}\\ \text{subject to} & \|\mathbf{w}\|^2=1\\ & \|\mathbf{w}-\mathbf{w}_0\|^2\le\xi\end{cases} \tag{28}$$

where $\psi_q\,(q=1,\cdots,Q)$ denotes the finite discrete doppler frequency in doppler interval Ω, the first constraint stands for the constant white noise gain of the doppler filter, $0\le\xi<2$ denotes the tolerance threshold that ensures the similarity between $\mathbf{w}$ and $\mathbf{w}_0$, $\mathbf{w}_0$ denotes the Wiener filter weight vector, which can maximize the output SINR at ψ_t and can be formulated as [35]

$$\mathbf{w}_0=\frac{(\mathbf{R}_c+\sigma_n^2\mathbf{I})^{-1}(\mathbf{s}\odot\mathbf{d}(\psi_t))}{\|(\mathbf{R}_c+\sigma_n^2\mathbf{I})^{-1}(\mathbf{s}\odot\mathbf{d}(\psi_t))\|^2}. \tag{29}$$

where ψ_t denotes the doppler frequency of the target according to the prior information and the aim of enforcing the similarity on $\mathbf{w}$ is to achieve better clutter mitigation performance like the Wiener filter.

However, the optimization problem (28) is nonconvex, since the objective function is nonconvex and the constraint $\|\mathbf{w}\|^2=1$ denotes a nonconvex set. Therefore, it's very hard to solve the optimization problem $\mathcal{P}$.

$$
\begin{aligned}
\mathbf{R}_c &= \mathbb{E}\{\mathbf{c}\mathbf{c}^H\} \qquad (25)\\
&= \mathbb{E}\left\{\sum_{r=1}^{N_c-1}\sum_{i=0}^{L-1}\sum_{p=1}^{N_c-1}\sum_{b=0}^{L-1}\alpha_{(r,i)}\alpha^*_{(p,b)}\mathbf{J}_r(\mathbf{b}(u_i)\odot\mathbf{d}(\psi_{(r,i)}))(\mathbf{b}(u_b)\odot\mathbf{d}(\psi_{(p,b)}))^H\mathbf{J}_p^T\right\}\\
&\quad+\mathbb{E}\left\{\sum_{i=0}^{L-1}\sum_{b=0}^{L-1}\alpha_{(0,i)}\alpha^*_{(0,b)}(\mathbf{b}(u_i)\odot\mathbf{d}(\psi_{(0,i)}))(\mathbf{b}(u_b)\odot\mathbf{d}(\psi_{(0,b)}))^H\right\}\\
&= \mathbb{E}\left\{\sum_{r=1}^{N_c-1}\sum_{i=0}^{L-1}|\alpha_{(r,i)}|^2\mathbf{J}_r(\mathbf{b}(u_i)\odot\mathbf{d}(\psi_{(r,i)}))(\mathbf{b}(u_i)\odot\mathbf{d}(\psi_{(r,i)}))^H\mathbf{J}_r^T\right\}+\mathbb{E}\left\{\sum_{i=0}^{L-1}|\alpha_{(0,i)}|^2(\mathbf{b}(u_i)\odot\mathbf{d}(\psi_{(0,i)}))(\mathbf{b}(u_i)\odot\mathbf{d}(\psi_{(0,i)}))^H\right\}\\
&= \sum_{r=1}^{N_c-1}\sum_{i=0}^{L-1}\mathbb{E}\{|\alpha_{(r,i)}|^2\}\mathbf{J}_r(\mathbf{b}(u_i)\mathbf{b}^H(u_i))\odot\mathbb{E}\{\mathbf{d}(\psi_{(r,i)})\mathbf{d}^H(\psi_{(r,i)})\}\mathbf{J}_r^T+\sum_{i=0}^{L-1}\mathbb{E}\{|\alpha_{(0,i)}|^2\}(\mathbf{b}(u_i)\mathbf{b}^H(u_i))\odot\mathbb{E}\{\mathbf{d}(\psi_{(0,i)})\mathbf{d}^H(\psi_{(0,i)})\}\\
&= \sum_{r=1}^{N_c-1}\sum_{i=0}^{L-1}\sigma_r^2\mathbf{J}_r\Gamma(\mathbf{b}(u_i),(r,i))\mathbf{J}_r^T+\sum_{i=0}^{L-1}\sigma_0^2\Gamma(\mathbf{b}(u_i),(0,i)),
\end{aligned}
$$

Let $\mathbf{W}\triangleq\mathbf{w}\mathbf{w}^H$ and $\mathbf{S}\triangleq\mathbf{s}\mathbf{s}^H$. The SINR can be recast equivalently as

$$
\begin{aligned}
\text{SINR}(\psi_q) &= \frac{|\alpha_t|^2|\mathbf{w}^H(\mathbf{s}\odot\mathbf{d}(\psi_q))|^2}{\mathbf{w}^H(\mathbf{R}_c+\sigma_n^2\mathbf{I})\mathbf{w}} \qquad (30)\\
&= \frac{|\alpha_t|^2(\mathbf{s}\odot\mathbf{d}(\psi_q))^H\mathbf{w}\mathbf{w}^H(\mathbf{s}\odot\mathbf{d}(\psi_q))}{\mathbf{w}^H(\mathbf{R}_c+\sigma_n^2\mathbf{I})\mathbf{w}}\\
&= \frac{|\alpha_t|^2\mathbf{d}^H(\psi_q)\left(\mathbf{w}\mathbf{w}^H\odot(\mathbf{s}\mathbf{s}^H)^*\right)\mathbf{d}(\psi_q)}{\mathbf{w}^H(\mathbf{R}_c+\sigma_n^2\mathbf{I})\mathbf{w}}\\
&= \frac{|\alpha_t|^2\mathbf{d}^H(\psi_q)(\mathbf{W}\odot\mathbf{S}^*)\mathbf{d}(\psi_q)}{\text{tr}\{(\mathbf{R}_c+\sigma_n^2\mathbf{I})\mathbf{W}\}}.
\end{aligned}
$$

The equation is true because of the identity $\mathbf{x}^H\mathbf{A}\mathbf{x}=\text{tr}\{\mathbf{A}\mathbf{X}\}$ where $\mathbf{X}=\mathbf{x}\mathbf{x}^H$ [36].

Therefore, the optimization problem (28) can be recast as

$$
\mathcal{P}_1\begin{cases}\max_{\mathbf{W}} & \min_{q=1,2,\cdots,Q}\ \frac{|\alpha_t|^2\mathbf{d}^H(\psi_q)(\mathbf{W}\odot\mathbf{S}^*)\mathbf{d}(\psi_q)}{\text{tr}\{(\mathbf{R}_c+\sigma_n^2\mathbf{I})\mathbf{W}\}}\\ \text{subject to} & \text{tr}\{\mathbf{W}\}=1\\ & \text{rank}(\mathbf{W})=1\\ & \mathbf{W}\succeq\mathbf{0}\\ & \text{tr}\{\mathbf{W}\mathbf{W}_0\}\geq\varepsilon\end{cases} \qquad (31)
$$

where $\mathbf{W}_0\triangleq\mathbf{w}_0\mathbf{w}_0^H$ and $\varepsilon\triangleq(\frac{2-\xi}{2})^2$.

However, $\mathcal{P}_1$ is still nonconvex, since the objective function is nonconvex and the constraint $\text{rank}(\mathbf{W})=1$ is nonconvex. We omit the constraint $\text{rank}(\mathbf{W})=1$ in $\mathcal{P}_1$ to obtain the relaxed optimization problem $\mathcal{P}_2$:

$$
\mathcal{P}_2\begin{cases}\max_{\mathbf{W}} & \min_{q=1,2,\cdots,Q}\ \frac{|\alpha_t|^2\mathbf{d}^H(\psi_q)(\mathbf{W}\odot\mathbf{S}^*)\mathbf{d}(\psi_q)}{\text{tr}\{(\mathbf{R}_c+\sigma_n^2\mathbf{I})\mathbf{W}\}}\\ \text{subject to} & \text{tr}\{\mathbf{W}\}=1\\ & \mathbf{W}\succeq\mathbf{0}\\ & \text{tr}\{\mathbf{W}\mathbf{W}_0\}\geq\varepsilon\end{cases} \qquad (32)
$$

where the constraints are all convex, however, the objective function is still nonconvex.

We introduce the slack variable $\tilde{t}\in\mathbb{R}$ and the optimization $\mathcal{P}_2$ can be recast equivalently as below

$$
\mathcal{P}_3\begin{cases}\max_{\mathbf{W},\tilde{t}} & \frac{\tilde{t}}{\text{tr}\{(\mathbf{R}_c+\sigma_n^2\mathbf{I})\mathbf{W}\}}\\ \text{subject to} & \text{tr}\{\mathbf{W}\}=1\\ & |\alpha_t|^2\mathbf{d}^H(\psi_q)(\mathbf{W}\odot\mathbf{S}^*)\mathbf{d}(\psi_q)\geq\tilde{t},\ \forall q\\ & \mathbf{W}\succeq\mathbf{0}\\ & \text{tr}\{\mathbf{W}\mathbf{W}_0\}\geq\varepsilon\end{cases} \qquad (33)
$$

According to Charnes-Cooper transform [37], we let $\mathbf{Y}=\zeta\mathbf{W}$ and $t=\zeta\tilde{t}$ for a auxiliary variable $\zeta\geq0$. The optimization $\mathcal{P}_3$ can be equivalently formulated as

$$
\mathcal{P}_4\begin{cases}\max_{\mathbf{Y},t,\zeta} & t\\ \text{subject to} & \text{tr}\{\mathbf{Y}\}=\zeta,\\ & |\alpha_t|^2\mathbf{d}^H(\psi_q)(\mathbf{Y}\odot\mathbf{S}^*)\mathbf{d}(\psi_q)\geq t,\ \forall q\\ & \text{tr}\{(\mathbf{R}_c+\sigma_n^2\mathbf{I})\mathbf{Y}\}=1\\ & \text{tr}\{\mathbf{Y}\mathbf{W}_0\}\geq\zeta\varepsilon\\ & \mathbf{Y}\succeq\mathbf{0}\\ & \zeta\geq0\end{cases} \qquad (34)
$$

Lemma 1: The optimization problems $\mathcal{P}_4$ and $\mathcal{P}_3$ are equivalent. What's more, the optimal values of the two problems are same, and the corresponding optimal solutions are one to one mapping.

Proof 1: Let $(\mathbf{W}_*,\tilde{t}_*)$ and $\upsilon(\mathcal{P}_3)$ are the optimal solution and optimal value of optimization problem $\mathcal{P}_3$, respectively. It can be checked easily that $(\mathbf{Y},t,\zeta)=(\frac{\mathbf{W}_*}{\text{tr}\{(\mathbf{R}_c+\sigma_n^2\mathbf{I})\mathbf{W}_*\}},\frac{\tilde{t}_*}{\text{tr}\{(\mathbf{R}_c+\sigma_n^2\mathbf{I})\mathbf{W}_*\}},\frac{1}{\text{tr}\{(\mathbf{R}_c+\sigma_n^2\mathbf{I})\mathbf{W}_*\}})$ is a feasible solution to optimization problem $\mathcal{P}_4$ and submit $(\mathbf{Y},t,\zeta)$ to (34), the value of the objective function is

$$
\frac{\tilde{t}_*}{\text{tr}\{(\mathbf{R}_c+\sigma_n^2\mathbf{I})\mathbf{W}_*\}}, \qquad (35)
$$

which is equal to the optimal value of optimization problem $\mathcal{P}_3$. Therefore, $\nu(\mathcal{P}_4)\geq\nu(\mathcal{P}_3)$.

Let $(\mathbf{Y}_*,t_*,\zeta_*)$ is the optimal solution of optimization problem $\mathcal{P}_4$. $\zeta_*>0$, otherwise $\mathbf{Y}=\mathbf{0}$, which is contradictory with $\text{tr}\{\mathbf{W}\}=1$. It can be checked easily that $(\frac{\mathbf{Y}_*}{\zeta_*},\frac{t_*}{\zeta_*})$ is a feasible solution to $\mathcal{P}_3$ and the corresponding value of the

objective function is t_*. Therefore, $\nu(\mathcal{P}_3) \geq \nu(\mathcal{P}_4)$. As a consequence, $\nu(\mathcal{P}_3) = \nu(\mathcal{P}_4)$ and $\mathcal{P}_3$ is equivalent to $\mathcal{P}_4$.

The optimization problem $\mathcal{P}_4$ is convex and can be solved using CVX toolbox.

V. THE SYNTHESIS STAGE

If the rank of $\mathbf{W}_*$ is one, $\mathbf{w}_*$ can be obtained by full rank decomposition [38], i.e., $\mathbf{W}_* = \mathbf{w}_*\mathbf{w}_*^H$. If the rank of $\mathbf{W}_*$ is bigger than one, the synthesis of $\mathbf{w}_*$ is much complicated. The rank-decomposition method is usually utilized to solve this problem.

The rank-one decomposition method can be described as below [39]:

Theorem 1: Suppose $\mathbf{W} \in \mathbb{C}^{N\times N}$ is a nonzero Hermitian positive semidefinite matrix (with $N \geq 3$) and $\{\mathbf{B}_1, \mathbf{B}_2, \mathbf{B}_3, \mathbf{B}_4\}$ are Hermitian matrices. Suppose that $(\text{tr}\{\mathbf{CB}_1\}, \text{tr}\{\mathbf{CB}_2\}, \text{tr}\{\mathbf{CB}_3\}, \text{tr}\{\mathbf{CB}_4\}) \neq (0,0,0,0)$ for any non-zero complex Hermitian positive semidefinite matrix $\mathbf{C}$. Then

- if $\text{rank}(\mathbf{W}) \geq 3$, then we can find a nonzero vector $\mathbf{w} \in \text{range}(\mathbf{W})$ in polynomial time so that

$$\mathbf{w}\mathbf{B}_i\mathbf{w}^H = \text{tr}\{\mathbf{W}\mathbf{B}_i\}, \quad i = 1,2,3,4; \tag{36}$$

- if $\text{rank}(\mathbf{W}) = 2$, for any $\mathbf{g} \notin \text{range}(\mathbf{W})$, there exists $\mathbf{y} \in \mathbb{C}^N$ in the linear subspace spanned by $\text{range}(\mathbf{W})$ and $\mathbf{g}$, so that

$$\mathbf{w}\mathbf{B}_i\mathbf{w}^H = \text{tr}\{\mathbf{W}\mathbf{B}_i\}, \quad i = 1,2,3,4; \tag{37}$$

Assume that $\mathbf{W}_*$ is an optimal solution to $\mathcal{P}_2$ and let

$$\psi_* = arg \min_{q=1,\cdots,Q} |\alpha_t|^2 |\mathbf{d}^H(\psi_q)(\mathbf{W}_* \odot \mathbf{S}^*)\mathbf{d}(\psi_q). \tag{38}$$

A feasible rank-one matrix $\mathbf{w}_*\mathbf{w}_*^H$ can be obtained so that

$$\text{tr}\left\{ \underbrace{(\mathbf{R}_c + \sigma_n^2\mathbf{I})}_{\mathbf{G}_1} \mathbf{W}_* \right\} = \mathbf{w}_*^H \mathbf{G}_1 \mathbf{w}_*, \tag{39}$$

and

$$\text{tr}\left\{ \underbrace{(\mathbf{S}^* \odot (\mathbf{d}(\psi_*)\mathbf{d}^H(\psi_*)))}_{\mathbf{G}_2} \mathbf{W}_* \right\} = \mathbf{w}_*^H \mathbf{G}_2 \mathbf{w}_*, \tag{40}$$

$$\text{tr}\left\{ \underbrace{(\mathbf{S}^* \odot (\mathbf{d}(\tilde{\psi})\mathbf{d}^H(\tilde{\psi})))}_{\mathbf{G}_3} \mathbf{W}_* \right\} = \mathbf{w}_*^H \mathbf{G}_3 \mathbf{w}_*,$$

$$\text{tr}\left\{ \underbrace{(\mathbf{S}^* \odot (\mathbf{d}(\bar{\psi})\mathbf{d}^H(\bar{\psi})))}_{\mathbf{G}_4} \mathbf{W}_* \right\} = \mathbf{w}_*^H \mathbf{G}_4 \mathbf{w}_*,$$

where $\bar{\psi}$ and $\tilde{\psi}$ are two arbitrary doppler frequency in doppler region of interest different from ψ_*. As a result, $\mathbf{w}_*$ can be obtained by $\mathbf{w}_* = \text{D}_1(\mathbf{W}, \mathbf{G}_1, \mathbf{G}_2, \mathbf{G}_3, \mathbf{G}_4)$ or $\mathbf{w}_* = \text{D}_2(\mathbf{W}, \mathbf{G}_1, \mathbf{G}_2, \mathbf{G}_3, \mathbf{G}_4)$ for cases where $\text{rank}(\mathbf{W}_*) \geq 3$ or $\text{rank}(\mathbf{W}_*) = 2$, respectively. Note that the condition $(\text{tr}(\mathbf{CG}_1), \text{tr}(\mathbf{CG}_2), \text{tr}(\mathbf{CG}_3), \text{tr}(\mathbf{CG}_4)) \neq (0,0,0,0)$ is satisfied [40].

VI. SIMULATION RESULTS

In this section, simulation results are presented to illustrate the benefits of the proposed method. The joint RadCom system is equipped with a 15-element ULA with an inter-element spacing of half-wavelength for transmit and an omnidirectional antenna for receive. The CPI consists of $N = 40$ pulses where the transmit weight vectors for each pulse is randomly selected from the specially designed set. As for the parameters of the clutter, the clutter power is set as $\sigma_0 = 50$dB and K_r is set as 1. The noise power is set as $\sigma_n^2 = 0$dB, the signal to noise ratio (SNR) is 10dB. We only consider the clutter located in $[-60°, 60°]$ where each range ring is divided into 100 discrete clutter patches, i.e., $L = 100$. What's more, ϵ is set as 0.008. The number of clutter range rings is set as $N_c = 2$ and ξ is set as 0.75. The normalized doppler frequency interval of interest is set as $\Omega = [0.384, 0.416]$ and the number of discrete doppler frequency is set as $Q = 5$. In the simulation, we assume the target, which normalized doppler frequency is 0.4, is located 0°. And the complex scattering coefficient of the target is set as $\alpha_t = 1$. A single communication receiver is located at $\theta_c = -50°$. The sidelobe region of radar is set as $\bar{\mathbf{\Theta}} = [-90°, -5°] \cup [5°, 90°]$, from which 36 discrete angle grids are uniformly selected. The dual step size is set as $\beta = 0.1$. $\mathbf{h}_k$, λ_i, μ_l and ν_m are initialized randomly. $\mathbf{z}_k$ is equal to $\mathbf{h}_k$. We assume that 1 bit of information is delivered in each radar pulse. For the AM based signalling strategy mentioned above, $\mathbf{h}_1$ and $\mathbf{h}_2$ are utilized to form the beampatterns whose the sidelobe level at communication direction are -24.4370dB, -27.9588dB, respectively.

Fig.2 shows the transmit power radiation pattern corresponding to AM based spatial modulation. The PSL of the designed beampattern is -12.4dB, which contributes to suppress the clutter in the radar sidelobe region.

Fig. 3 shows the modulus of every element of weight vector $\mathbf{h}_1$ and $\mathbf{h}_2$. As shown in the figure, $\mathbf{h}_1$ and $\mathbf{h}_2$ grantee the constant modulus of the radar waveforms for joint RadCom systems based on spatial modulation.

Fig. 4 shows the output SINR versus normalized doppler frequency under different coherent pulse length N for both non spatial modulation and spatial modulation. As shown in the picture, the increase of the coherent pulse number N causes the SINR increase of both proposed doppler filter and Wiener filter. However, the increase of N causes the robustness of Wiener filter degrade greatly. On the contrary, the proposed doppler filter still keep robust.

Fig. 5 shows the output SINR versus normalized doppler frequency under different doppler intervals Ω for both non spatial modulation and spatial modulation. We consider $\Omega = [0.36, 0.44]$, $\Omega = [0.368, 0.432]$, $\Omega = [0.376, 0.424]$ respectively. As shown in the picture, the proposed doppler filter keeps robust in all these all doppler intervals. What's more, the bigger doppler interval, the worse robustness of the Wiener filter.

Fig. 6 shows the output SINR versus normalized doppler frequency under different similarity constraints ξ for both non spatial modulation and spatial modulation. we consider $\xi = 0.5$, $\xi = 0.75$ and $\xi = 1$ respectively. As shown in the figure,

the less ξ is, the more similarity between proposed robust doppler filter and the Wiener filter is. However, the robustness of the proposed robust doppler filter degrades.

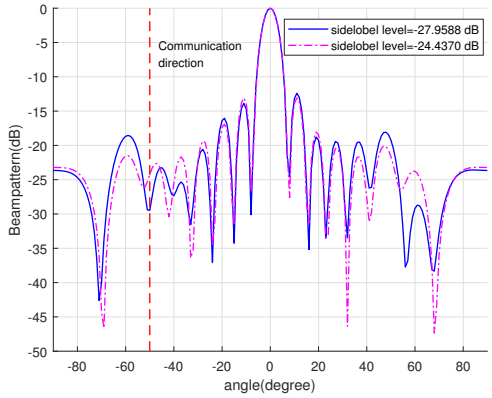

Fig. 2. Transmit power radiation pattern corresponding to AM based spatial modulation

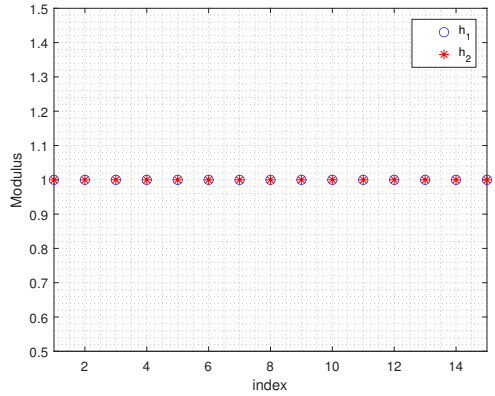

Fig. 3. Modulus of weight vectors for beampatterns of joint RadCom systems based on spatial modulation.

VII. CONCLUSION

In this paper, we designed the beamforming weight vectors for joint RadCom systems based on spatial modulation under constant modulus constraint. We proposed a method based on ADMM to solve the nonconvex optimization problem. What's more, we analysed the effect of spatial modulation on clutter mitigation. The joint RadCom systems based on spatial modulation introduced variations in radar beampatterns and cause clutter modulation problem. Considering the doppler frequency mismatch due to all kinds of reasons, we aimed to design the robust doppler filter for joint RadCom systems to maximize the worst SINR of the doppler filter in a specific doppler shift interval of interest. We relaxed the nonconvex problem to a SDP to obtain a suboptimal solution. Taking the Wiener filter as a reference, lots of simulation results showed the proposed doppler filter are more robust than Wiener filter.

REFERENCES

[1] L. Zheng, M. Lops, Y. C. Eldar, and X. Wang, "Radar and communication coexistence: An overview: A review of recent methods," *IEEE Signal Processing Magazine*, vol. 36, no. 5, pp. 85–99, 2019.

[2] K. V. Mishra, M. R. Bhavani Shankar, V. Koivunen, B. Ottersten, and S. A. Vorobyov, "Toward millimeter-wave joint radar communications: A signal processing perspective," *IEEE Signal Processing Magazine*, vol. 36, no. 5, pp. 100–114, 2019.

[3] A. Hassanien, M. G. Amin, E. Aboutanios, and B. Himed, "Dual-function radar communication systems: A solution to the spectrum congestion problem," *IEEE Signal Processing Magazine*, vol. 36, no. 5, pp. 115–126, 2019.

[4] F. Liu, L. Zhou, C. Masouros, A. Lit, W. Luo, and A. Petropulu, "Dual-functional cellular and radar transmission: Beyond coexistence," in *2018 IEEE 19th International Workshop on Signal Processing Advances in Wireless Communications (SPAWC)*, 2018, pp. 1–5.

[5] D. Ma, N. Shlezinger, T. Huang, Y. Liu, and Y. C. Eldar, "Joint radar-communication strategies for autonomous vehicles: Combining two key automotive technologies," *IEEE Signal Processing Magazine*, vol. 37, no. 4, pp. 85–97, 2020.

[6] W. Yuan, F. Liu, C. Masouros, J. Yuan, and D. W. Kwan Ng, "Joint radar-communication-based bayesian predictive beamforming for vehicular networks," in *2020 IEEE Radar Conference (RadarConf20)*, 2020, pp. 1–6.

[7] A. Hassanien, M. G. Amin, Y. D. Zhang, and F. Ahmad, "Signaling strategies for dual-function radar communications: an overview," *IEEE Aerospace and Electronic Systems Magazine*, vol. 31, no. 10, pp. 36–45, 2016.

[8] T. Huang, N. Shlezinger, X. Xu, Y. Liu, and Y. C. Eldar, "Majorcom: A dual-function radar communication system using index modulation," *IEEE Transactions on Signal Processing*, vol. 68, pp. 3423–3438, 2020.

[9] T. Huang, X. Xu, Y. Liu, N. Shlezinger, and Y. C. Eldar, "A dual-function radar communication system using index modulation," in *2019 IEEE 20th International Workshop on Signal Processing Advances in Wireless Communications (SPAWC)*, 2019, pp. 1–5.

[10] J. Xu and X. Wang, "Joint radar-communication system design via fh code selection and psk modulation," in *2019 IEEE International Conference on Signal, Information and Data Processing (ICSIDP)*, 2019, pp. 1–5.

[11] X. Wang and A. Hassanien, "Phase modulated communications embedded in correlated fh-mimo radar waveforms," in *2020 IEEE Radar Conference (RadarConf20)*, 2020, pp. 1–6.

[12] X. Wang, A. Hassanien, and M. G. Amin, "Dual-function mimo radar communications system design via sparse array optimization," *IEEE Transactions on Aerospace and Electronic Systems*, vol. 55, no. 3, pp. 1213–1226, 2019.

[13] A. Hassanien, M. G. Amin, Y. D. Zhang, F. Ahmad, and B. Himed, "Non-coherent psk-based dual-function radar-communication systems," in *2016 IEEE Radar Conference (RadarConf)*, 2016, pp. 1–6.

[14] A. Hassanien, M. G. Amin, Y. D. Zhang, and B. Himed, "A dual-function mimo radar-communications system using psk modulation," in *2016 24th European Signal Processing Conference (EUSIPCO)*, 2016, pp. 1613–1617.

[15] A. Ammar, Y. D. Zhang, and Y. Gu, "Dual-function radar-communications using qam-based sidelobe modulation," *Digital Signal Processing*, vol. 82, pp. 166–174, 2018.

[16] D. Ma, N. Shlezinger, T. Huang, Y. Shavit, M. Namer, Y. Liu, and Y. Eldar, "Spatial modulation for joint radar-communications systems: Design, analysis, and hardware prototype," *IEEE Transactions on Vehicular Technology*, pp. 1–1, 2021.

[17] C. Sahin, J. Jakabosky, P. M. McCormick, J. G. Metcalf, and S. D. Blunt, "A novel approach for embedding communication symbols into physical radar waveforms," in *2017 IEEE Radar Conference (RadarConf)*, 2017, pp. 1498–1503.

[18] A. Hassanien, M. G. Amin, Y. D. Zhang, and F. Ahmad, "Dual-function radar-communications: Information embedding using sidelobe control and waveform diversity," *IEEE Transactions on Signal Processing*, vol. 64, no. 8, pp. 2168–2181, 2016.

[19] A. Hassanien, B. Himed, and B. D. Rigling, "A dual-function mimo radar-communications system using frequency-hopping waveforms," in *2017 IEEE Radar Conference (RadarConf)*, 2017, pp. 1721–1725.

[20] A. De Maio, S. De Nicola, Y. Huang, Z. Luo, and S. Zhang, "Design of phase codes for radar performance optimization with a similarity constraint," *IEEE Transactions on Signal Processing*, vol. 57, no. 2, pp. 610–621, 2009.

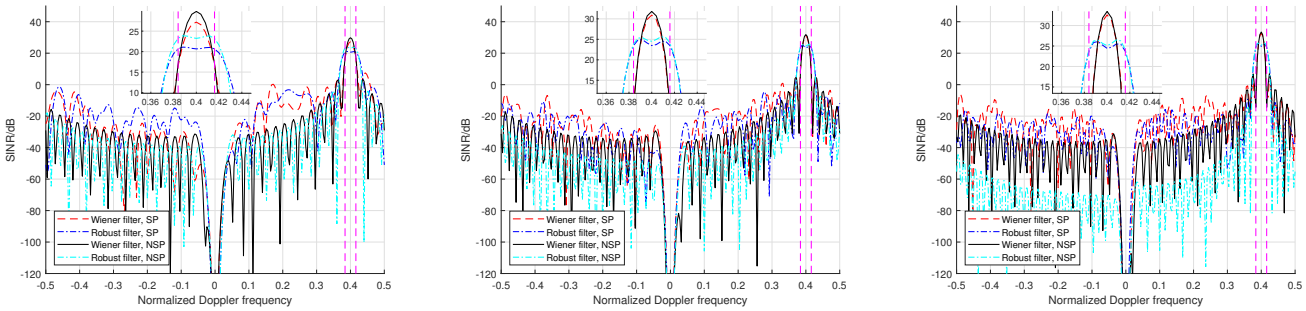

(a) $\xi = 0.75, N = 40, \Omega = [0.384, 0.416]$ (b) $\xi = 0.75, N = 50, \Omega = [0.384, 0.416]$ (c) $\xi = 0.75, N = 60, \Omega = [0.384, 0.416]$

Fig. 4. Output SINR versus normalized doppler frequency under coherent pulse length N

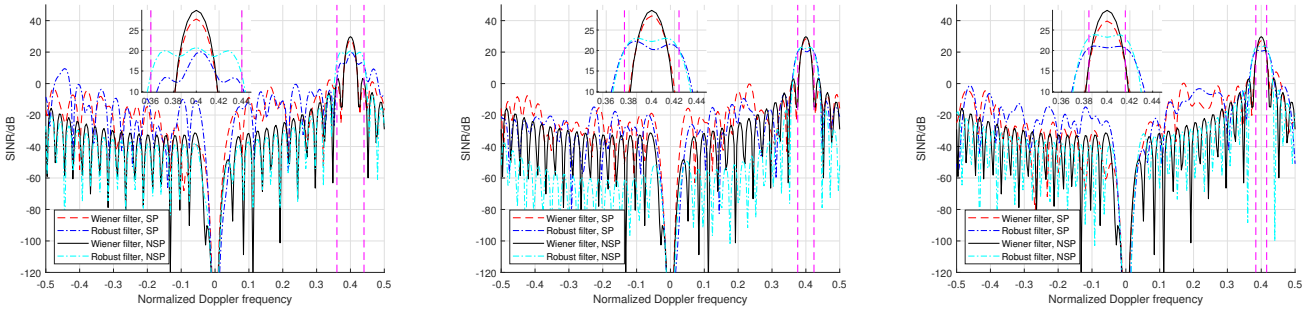

(a) $\xi = 0.75, N = 40, \Omega = [0.36, 0.44]$ (b) $\xi = 0.75, N = 40, \Omega = [0.376, 0.424]$ (c) $\xi = 0.75, N = 40, \Omega = [0.384, 0.416]$

Fig. 5. Output SINR versus normalized doppler frequency under different doppler interval of interest

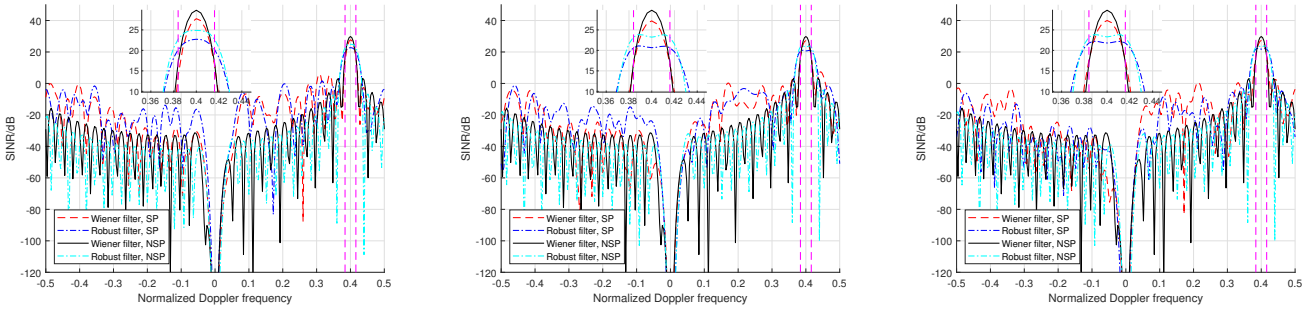

(a) $\xi = 0.5, N = 40, \Omega = [0.384, 0.416]$ (b) $\xi = 0.75, N = 40, \Omega = [0.384, 0.416]$ (c) $\xi = 1, N = 40, \Omega = [0.384, 0.416]$

Fig. 6. Output SINR versus normalized doppler frequency under different similarity constraint

[21] Z. Lin, W. Pu, and Z. Q. Luo, "Minimax design of constant modulus mimo waveforms for active sensing," *IEEE Signal Processing Letters*, vol. 26, no. 10, pp. 1531–1535, 2019.

[22] W. Fan, J. Liang, and J. Li, "Constant modulus mimo radar waveform design with minimum peak sidelobe transmit beampattern," *IEEE Transactions on Signal Processing*, vol. 66, no. 16, pp. 4207–4222, 2018.

[23] T. Huang, N. Shlezinger, X. Xu, Y. Liu, and Y. C. Eldar, "Majorcom: A dual-function radar communication system using index modulation," *IEEE Transactions on Signal Processing*, vol. 68, pp. 3423–3438, 2020.

[24] S. D. Blunt, M. R. Cook, and J. Stiles, "Embedding information into radar emissions via waveform implementation," in *2010 International Waveform Diversity and Design Conference*, 2010, pp. 000 195–000 199.

[25] A. Aubry, A. DeMaio, A. Farina, and M. Wicks, "Knowledge-aided (potentially cognitive) transmit signal and receive filter design in signal-dependent clutter," *IEEE Transactions on Aerospace and Electronic Systems*, vol. 49, no. 1, pp. 93–117, 2013.

[26] A. Aubry, A. D. Maio, Y. Huang, and M. Piezzo, "Robust design of radar doppler filters," *IEEE Transactions on Signal Processing*, vol. 64, no. 22, pp. 5848–5860, 2016.

[27] A. Aubry, A. De Maio, and M. M. Naghsh, "Optimizing radar waveform and doppler filter bank via generalized fractional programming," *IEEE Journal of Selected Topics in Signal Processing*, vol. 9, no. 8, pp. 1387–1399, 2015.

[28] M. M. Naghsh, M. Soltanalian, P. Stoica, M. Modarres-Hashemi, A. De Maio, and A. Aubry, "A doppler robust design of transmit sequence and receive filter in the presence of signal-dependent interference," *IEEE Transactions on Signal Processing*, vol. 62, no. 4, pp. 772–785, 2014.

[29] X. Du, A. Aubry, A. De Maio, and G. Cui, "Hidden convexity in robust waveform and receive filter bank optimization under range unambiguous clutter," *IEEE Signal Processing Letters*, vol. 27, pp. 885–889, 2020.

[30] X. Zhang, X. Wang, and E. Aboutanios, "Effect analysis of spatial modulation on clutter mitigation for joint radcom systems and solutions," in *2020 IEEE Radar Conference (RadarConf20)*, 2020, pp. 1–6.

[31] J. Li, P. Stoica, L. Xu, and W. Roberts, "On parameter identifiability of mimo radar," *IEEE Signal Processing Letters*, vol. 14, no. 12, pp. 968–971, 2007.

[32] J. Ward, "Space-time adaptive processing for airborne radar," 1998.
[33] M. A. Richards, J. A. Scheer, and W. A. Holm, "Principles of modern radar: Basic principles," *IET Digital Library*, 2010.
[34] W. L. Melvin, "A stap overview," *IEEE Aerospace and Electronic Systems Magazine*, vol. 19, no. 1, pp. 19–35, 2004.
[35] S. A. Vorobyov, A. B. Gershman, and Zhi-Quan Luo, "Robust adaptive beamforming using worst-case performance optimization: a solution to the signal mismatch problem," *IEEE Transactions on Signal Processing*, vol. 51, no. 2, pp. 313–324, 2003.
[36] R. Bhatia, *Matrix analysis*. Matrix Analysis, 1996.
[37] A. Zappone and E. Jorswieck, "Energy efficiency in wireless networks via fractional programming theory," *Found. Trends Commun. Inf. Theory*, vol. 11, no. 3–4, p. 185–396, Jun. 2015. [Online]. Available: https://doi.org/10.1561/0100000088
[38] G. Golub and A. Loan, "Matrix computations," *mathematical gazette*, 1986.
[39] W. Ai, Y. Huang, and S. Zhang, "New results on hermitian matrix rank-one decomposition," *Mathematical Programming*, vol. 128, no. 1-2, pp. 253–283, 2011.
[40] A. De Maio, Y. Huang, D. P. Palomar, S. Zhang, and A. Farina, "Fractional qcqp with applications in ml steering direction estimation for radar detection," *IEEE Transactions on Signal Processing*, vol. 59, no. 1, pp. 172–185, 2011.